# High-pressure structure and electronic transport in hole-doped $La_{3/4}Ca_{1/4}MnO_3$ perovskites

C. Meneghini,[1,2] D. Levy,[3] S. Mobilio,[2,4] M. Ortolani,[5] M. Nuñez-Reguero,[6] Ashwani Kumar,[7] and D. D. Sarma[7]
[1]*INFM c/o GILDA-ESRF, Avenue des Martyrs, BP 220, F-38043 Grenoble Cedex, France*
[2]*Dip. di Fisica E. Amaldi, Universitá di Roma Tre, via della Vasca Navale 84, I-00146 Roma, Italy*
[3]*Dip. di Science Mineralogiche e petrologiche, Universitá di Torino, Via V. Caruso 25, I-0125 Torino, Italy*
[4]*Laboratori Nazionali di Frascati, INFM, P.O. Box 13, I-00044 Frascati, Italy*
[5]*Dip. di Fisica, Universitá di Roma "La Sapienza," Piazzale A. Moro 2, I-00185 Roma, Italy*
[6]*CRTBT/CNRS, BP166 cedex 09, F-38042 Grenoble, France*
[7]*Solid State and Structural Chemistry Unit, Indian Institute of Science, Bangalore 560 012, India*
(Received 29 May 2001; published 13 December 2001)

The structure and electronic transport properties of hole-doped $La_{3/4}Ca_{1/4}MnO_3$ perovskite have been investigated as a function of pressure up to about 15 GPa. Though the applied pressure enhances the electrical conductivity, the high-pressure resistivity data point out a competing mechanism interfering with the pressure-induced charge delocalization that prevent the system from reaching a fully metallic state around room temperature. X-ray diffraction results reveal unexpected structural modifications with increasing pressure that can be interpreted with changes in the coherence length of the Jahn-Teller distortions.

DOI: 10.1103/PhysRevB.65.012111 PACS number(s): 62.50.+p, 61.10.−i, 75.30.Vn, 72.80.−r

Mixed valence manganese oxide perovskites, with the general formula $A_{1-x}B_xMnO_3$ (where $A$ is a rare-earth atom and $B$ a divalent metal), have been the subject of intensive theoretical and experimental investigations due to their remarkable magnetotransport properties. For a range of compositions, these compounds are ferromagnetic metals at low temperature and become paramagnetic insulators at high temperatures. Some compounds (like $La_{1-x}Ca_xMnO_3$ with $0.2<x<0.5$) have the metal-to-insulator (MI) transition temperature $T_{MI}$ close and coupled to the Curie temperature $T_c$, producing a characteristic sharp resistivity drop on cooling below $T_c$. The application of an external magnetic field strongly enhances the electrical conductivity near the transition, giving rise to the so-called colossal magnetoresistance (CMR) effect.[1] The phase diagram in the space of magnetic and electronic transport properties widely changes as a function of parameters like pressure, applied magnetic field, and composition, pointing out a close and complex interplay between structure, charge transport, and magnetism. The proposed theories principally rely on the competition between the double-exchange (DE) mechanism,[2–5] favoring the ferromagnetic metallic state, and a charge-lattice coupling (polaronic mechanism) which is related to the Jahn-Teller (JT) effect on the $Mn^{3+}$ and reduces the charge mobility in the high-temperature insulating phase.[6,7] As a matter of fact, several theoretical and experimental works[8–20] have demonstrated the close connection between the evolution of structural distortions and changes in the magnetotransport properties, definitively proving that the local JT distortions have a dominant role for the localization of charge carriers in the insulating phase.

Pressure ($P$) is a fundamental thermodynamic variable, which affects both the volume of the cell and the local structure, substantially modifying the magnetotransport properties.[21–26] Thus investigations under high pressure may give further information about the delicate balance between structure, magnetism, and electron mobility. It has been observed that applied pressure or magnetic field ($H$) produce qualitatively similar effects[21,23,26] in that both stabilize the ferromagnetic metallic state. However, the mechanisms through which $P$ and $H$ favor charge mobility are very different: $H$, favoring the spin alignment between Mn neighbors, enhances the bandwidth of itinerant $e_g$ electrons and, therefore, the mobility via the DE mechanism. On the contrary, $P$ enhances the bandwidth directly by modifying the Mn-O bond length and Mn-O-Mn bond angle distributions.[11,24] Moreover, changes in the self-trapping energy as a function of $P$ have also been postulated.[22] Several studies confirmed the increase in $T_c$ ($T_{MI}$) as a function of applied pressure, evidencing the shift of the energy balance in favor of delocalization over the polaronic localization. This lead to the belief that at high enough pressures, the $T_{MI}$ would be sufficiently high to make the system metallic at room temperature (RT). It has been observed[22] that the effect of applied hydrostatic pressure on the magnetotransport properties can be reproduced by changing the size of the metal ions, i.e., through the so-called internal or chemical pressure $P_c$. On the basis of this analogy a complete metalization at RT is expected around 5–6 GPa in $La_{3/4}Ca_{1/4}MnO_3$. In contrast to this belief transport measurements up to a pressure of about 1.7 GPa show that the pressure coefficient $dT_c/dP$ systematically decreases with $P$ and point to a saturation effect in the enhancement of ferromagnetic metallic state[21] at $P\sim 2$ GPa. Moreover, recent high-pressure spectroscopic studies[27,28] observed anomalous and unexpected features in the Raman spectra on raising the pressure above 6–7 GPa that are in contrast to the hypothesis of a pressure-induced insulator-to-metal transition around RT. These results suggest the presence of a progressive charge localization mechanism interfering with the metalization process with increasing $P$. However, the origin of such a mechanism is not yet understood. Further, there are no direct measurements of electronic transport or structural properties at higher pressures.

The present work investigates the evolution of electrical conductivity and structural properties of a $La_{3/4}Ca_{1/4}MnO_3$

 

hole-doped perovskite in the high-pressure region, up to about 15 GPa, in order to address these issues directly. Our results point out a saturation effect in the pressure enhancement of electrical conductivity that prevents the metalization of the system near RT. X-ray diffraction (XRD) data show that an unexpected increase in coherent JT distortions is related to the strengthening of the charge localization at high pressures.

Powders of $La_{3/4}Ca_{1/4}MnO_3$ were prepared by the conventional solid-state method using pure $La_2O_3$, $CaCO_3$, and $Mn_3O_4$ precursors. The sample was characterized at room pressure (RP) by resistivity, ac susceptibility, magnetoresistance, x-ray absorption spectroscopy,[16] Raman,[27] and IR (Ref. 28) spectroscopies. The sample exhibits $T_{MI}$ ($T_c$) around 220 K [Fig. 1(c)] at $P=1$ bar. High-pressure resistivity was measured using a standard four-probe method at the CRTBT/CNRS (Grenoble, France) in a sintered diamond-pyrophillite anvil cell.[29] Quasihydrostatic pressure was obtained by using steatite as a pressure medium[30] and was calibrated by monitoring the superconducting transition temperature of a lead sample.

Isobaric $R(P,T)$ curves were obtained on heating the sample between ~190 and ~380 K with a sampling step of about 0.1 K. The high-pressure XRD experiments were performed on the ID9 beamline at ESRF (Grenoble, France) using an angle-dispersed setup designed for accurate high-pressure XRD diffraction experiments. High pressure was achieved using a diamond anvil cell (DAC) with 600 $\mu$m diameter and XRD patterns were recorded using an imaging plate ($400\times400\,mm^2$) camera with $100\times100\,\mu m^2$ pixel dimension. The diamonds, mounted with a thrust axis parallel to the incident beam, allowed us to collect a diffraction cone of about 25° in $2\theta$. The pressure on the sample was determined before and after each imaging, by monitoring the fluorescence line shift of a small ruby crystal enclosed in the DAC with the sample.[31] Powder of $La_{3/4}Ca_{1/4}MnO_3$ sample were enclosed in a pinhole steel gasket, and $N_2$ was used as a hydrostatic pressure medium. XRD patterns were collected at room temperature in the pressure range 0–14 GPa with steps of about 1 GPa. The collected two-dimensional (2D) XRD images were treated and integrated using the FIT2D (Ref. 32) package and the structural refinement of integrated patterns was achieved through the Rietveld method as implemented in the GSAS software package.[33]

In Fig. 1(a) we show the isobaric $R(P,T)$ curves, while in Fig. 1(b) we report the derivative of $R$ with respect to temperature, $dR/dT$, for $P\geqslant3$ GPa curves. From these figures it is clear that the applied pressure enhances the electrical conductivity in the whole temperature and pressure range investigated. At lower pressures ($P\leqslant1.4$ GPa) the pressure-induced shift of $T_{MI}$ is evident with a slope $dT_{MI}/dP \sim10$ K/GPa. On raising $P$ above 1.4 GPa the resistivity peak signaling the MI transition disappears and the system clearly remains insulator ($dR/dT<0$) in the whole temperature range investigated [Figs. 1(a) and 1(b)]. These results clearly and directly demonstrate that the hydrostatic pressure enhances the electrical conductivity, but never brings the system into a metallic state at RT. This result allows us to definitively exclude a pressure induced MI transition at room

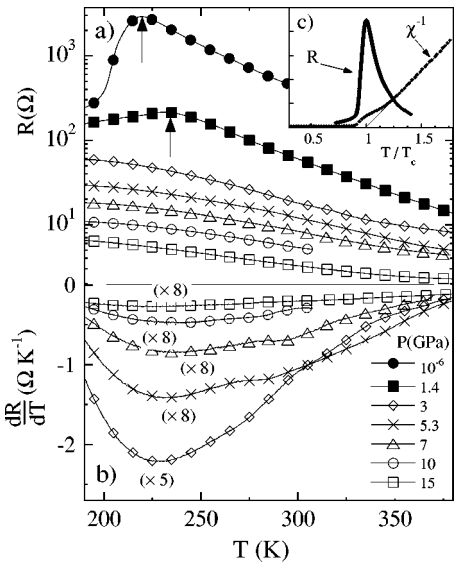


FIG. 1. (a) High-pressure electrical resistance and (b) its temperature derivative (for $P\geqslant3$ GPa data) as a function of temperature for $La_{3/4}Ca_{1/4}MnO_3$. Magnetic susceptibility ($\chi^{-1}$) and resistivity ($R$) measured at room pressure are displayed in panel (c).

temperature in contrast to the expectation based on the equivalence between hydrostatic and chemical pressure. The absence of this MI transition in $P\geqslant3$ GPa points out the presence of a charge localization mechanism interfering with the pressure-induced charge delocalization effect.

The structural refinement of XRD patterns for $La_{3/4}Ca_{1/4}MnO_3$ was performed on the basis of the *Pnma* space group (No. 62) in accordance with published literature.[11] Such a structure derives from the ideal cubic perovskite structure, being made of two pseudocubic units superimposed along the $b$ axis; the $MnO_6$ octahedra are located on the pseudocube corners, while the La/Ca randomly occupy the cube centers. The lattice parameters are related to the edge of the ideal cubic perovskite $a_p$ by $a\sim c\sim a_p\sqrt{2}$ and $b=2a_p$. The structure of undoped $LaMnO_3$ ($x=0$) is characterized by two kinds of distortions. The first one is due to the tilting of $MnO_6$ octahedra, originating from the size mismatch between the $La^{3+}$ ion and free space at the center of pseudocubic units. The other is the JT distortion of the $Mn^{3+}O_6$ octahedra that produces three pairs of Mn-O bond, one ($Mn\text{-}O_\perp$) for the apical bonds along the $b$ axis, and two ($Mn\text{-}O_\parallel$) for bonds in the $ac$ in plane. In doped compounds ($x>0.2$) the long-range coherence of JT distortions is negligible, but they remain large locally, at least in the paramagnetic (PM) insulating state.[18] In Fig. 2, we show a typical XRD pattern recorded at $P=5.8$ GPa and its Rietveld refinement. A very good agreement between the experimental data and its Rietveld refinement is evident from the low value of residual also shown in the same figure. In the inset of Fig. 2, a selected region of XRD patterns, involving 400, 424, and 004 Bragg peaks at various pressures, is reported to highlight the pressure-induced modifications in the structure of this compound. The main peak at ~19° shifts to higher angles with increasing pressure, indicating a volume compression as the pressure is increased to 14 GPa. Further, a shoulder ap-

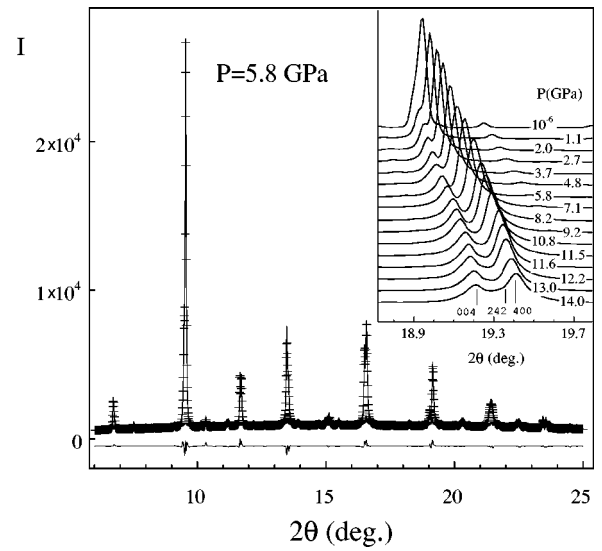


FIG. 2. XRD pattern for $La_{3/4}Ca_{1/4}MnO_3$ at 5.8 GPa (cross) with its Rietveld refinement (solid line) and residual (shifted for clarity). In the inset, XRD patterns in the region of 400, 424, and 004 Bragg peaks as a function of the applied pressure are shown.

pears to this main peak at a pressure of ~1.1 GPa, which develops into a main peak at higher pressures, pointing out the evolution of the structure to a less symmetric one which may be related to different compression along the three crystallographic axes.

The data reported in Fig. 3 allow us to quantify the effect of $P$ on the main structural parameters. In Fig. 3(a) the cell volume $V(P)$ is reported. It monotonically decreases with pressure, indicating a global contraction of the cell as a function of the applied pressure. The solid line represents the

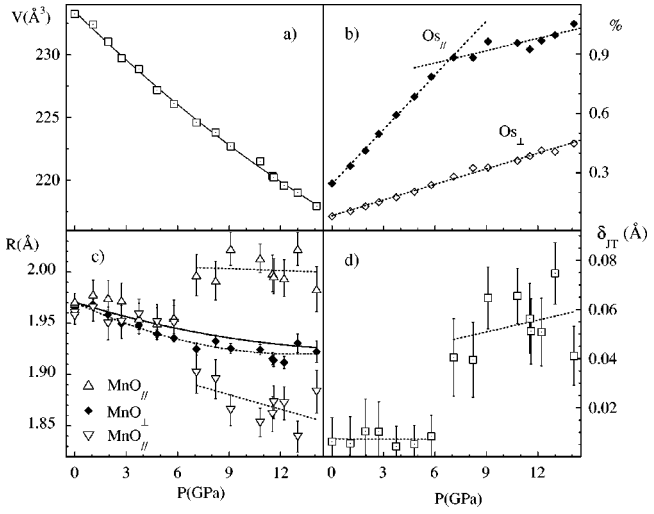


FIG. 3. Evolution of various structural parameters as a function of the applied pressure in $La_{3/4}Ca_{1/4}MnO_3$. (a) Cell volume (squares) fitted with the Birch-Murneghan equation of state (solid line). (b) Orthorombic strain (see text). (c) Mn-O bond lengths; the solid lines depict the evolution of the average Mn-O bond length. (d) coherent Jahn-Teller distortion. In panels (b), (c), and (d) dashed lines are a guide for the eyes.

fitting with the Birch-Murnegan[34] equation from which the bulk modulus $K=178$ and its derivative $K'=4$ are obtained. Figure 3(b) shows ''orthorhombic strains'' in the *ac* plane, which is defined as $Os_{\parallel}=2(c-a)/(c+a)$, and along the *b* axis with respect to the *ac* plane: $Os_{\perp}=2(a+c-b\sqrt{2})/(a+c+b\sqrt{2})$. $Os_{\parallel}$ and $Os_{\perp}$ represent the departure of the cell edges from those of an ideal cubic lattice in which $Os_{\perp}=Os_{\parallel}=0$. The room pressure $Os_{\parallel}(\mathrm{RP})\approx 2.5\times 10^{-3}$ and $Os_{\perp}(\mathrm{RP})\approx 0.8\times 10^{-3}$ are in agreement with those deducible from the data reported in the literature[11] for similar compounds ($Os_{\parallel}\approx 3.2\times 10^{-3}$ and $Os_{\perp}\approx 0.9\times 10^{-3}$) and about one order of magnitude lower than the values measured on undoped $LaMnO_3$ ($Os_{\parallel}>3\times 10^{-2}$ and $Os_{\perp}\approx 1.6\times 10^{-2}$). On increasing the pressure both $Os_{\parallel}$ and $Os_{\perp}$ increase, indicating an overall reinforcement of the orthorhombic nature of the lattice. Further, while the $Os_{\perp}$ evolves almost linearly with increasing $P$, $Os_{\parallel}$ deviates from a linear behavior around $P^*=6-7$ GPa. It is worthwhile to notice that the observed trend on $Os_{\parallel}(P)$ closely tracks the pressure dependence of the Raman peak associated with the in-plane stretching mode of oxygen octahedron ($B_{2g}\sim 630\,\mathrm{cm}^{-1}$).[27]

The evolution of Mn-O bond lengths as a function of $P$ is reported in Fig. 3(c). At low pressures ($P<P^*$), the three Mn-O bond lengths, almost indistinguishable within the accuracy of the data, roughly decrease with $P$. However, on raising $P$ above $P^*$ the Mn-O bond lengths split, pointing out three distinct distances. It is worthwhile to notice that, despite the uncertainty in Mn-O bond lengths, all the patterns collected at $P>P^*$ depict a similar splitting that is absent in the patterns collected at lower pressure. This systematic effect cannot be ascribed to a simple statistical uncertainty. The splitting of Mn-O bond lengths is surprising, if not completely unexpected, since the extrapolation of the low-pressure structural data and the analogy with chemical-pressure data suggested an overall reduction of the structural distortions as a function of $P$, bringing the system towards a more symmetric phase, typical of a metallic phase. On the contrary the observed splitting of Mn-O bond lengths for $P>P^*$ points out the appearance of an additional coherent distortion of the $MnO_6$ octahedra. In Fig. 3(d) we report the amplitude of the coherent Jahn-Teller distortion calculated as $\delta_{\mathrm{JT}}=\sqrt{(1/N)\Sigma_i^N(R^i_{\mathrm{MnO}}-\overline{R_{\mathrm{MnO}}})^2}$. At low pressure the weak $\delta_{\mathrm{JT}}<10^{-2}$ Å are in agreement, within the statistical accuracy, with published $\delta_{\mathrm{JT}}(\mathrm{RP})\approx 3\times 10^{-3}$ Å.[11] Raising the pressure above $P^*$, $\delta_{\mathrm{JT}}$ rapidly increases to a value of $\sim 6\times 10^{-2}$ Å. This abrupt change in JT distortions at $P^*$ is in agreement with recent high-pressure Raman spectroscopy results,[27] which suggested that such an abrupt change is due to pressure-induced modifications of the charge to lattice coupling.

In Fig. 3, it is remarkable to notice the smoothness of $V(P)$ in the region around 7 GPa, in evident contrast to the features observed in the other parameters and in particular with the sharp splitting of the Mn-$O_{\parallel}$ distances. Further, the absence of superlattice peaks in the higher-pressure diffraction patterns allows one to exclude the presence of a superstructure, changing the lattice periodicity. This finding can be explained as due to a structural modification in which the JT

distortions of the $MnO_6$ octahedra do not change their magnitude, but only modify their coherence length, going from totally incoherent (local and/or dynamical JT distortions) at low pressure to a long-range coherent one at high pressures. It is worthwhile to notice that the magnitude of the coherent $\delta_{JT}$ reported here in the high-pressure region is of the same order of that deducible from extended x-ray absorption fine structure (EXAFS) measurements in the paramagnetic phase at $P=1$ bar.[18] This supports and strengthens the above interpretation.

To summarize, our high-pressure transport and structural results definitively deny the equivalence between internal and hydrostatic pressure and provide direct evidence for different competing mechanisms that affect the charge transport in manganites as a function of applied pressure. While in the low-pressure regime ($P<7$ GPa) the applied pressure promotes the charge delocalization and the metallic state, at higher pressures a charge localization effect grows up, preventing the realization of the metallic state of the system at room temperature.


[1] R. von Helmolt *et al.*, Phys. Rev. Lett. **71**, 2331 (1993).
[2] C. Zener, Phys. Rev. **82**, 403 (1951).
[3] P. Anderson and H. Hasegawa, Phys. Rev. **100**, 675 (1955).
[4] P. de Gennes, Phys. Rev. **118**, 141 (1960).
[5] K. Kubo and A. A. Ohata, J. Phys. Soc. Jpn. **33**, 21 (1972).
[6] A. J. Millis, P. B. Littlewood, and B. I. Shraiman, Phys. Rev. Lett. **74**, 5144 (1995).
[7] A. J. Millis, B. I. Shraiman, and R. Mueller, Phys. Rev. Lett. **77**, 175 (1996).
[8] H. Roder, J. Zhang, and A. R. Bishop, Phys. Rev. Lett. **76**, 1356 (1996).
[9] D. Louca and T. Egami, Phys. Rev. B **59**, 6193 (1999).
[10] P. G. Radaelli *et al.*, Phys. Rev. Lett. **75**, 4488 (1996).
[11] P. G. Radaelli *et al.*, Phys. Rev. B **56**, 8265 (1997).
[12] K. H. Kim, J. H. Jung, and T. W. Noh, Phys. Rev. Lett. **81**, 1517 (1998).
[13] C. H. Booth, F. Bridges, G. J. Snyder, and T. H. Geballe, Phys. Rev. B **54**, 15 606 (1998).
[14] C. H. Booth *et al.*, Phys. Rev. B **57**, 10 440 (1998).
[15] C. Meneghini *et al.*, Phys. Rev. B **56**, 3520 (1997).
[16] C. Castellano *et al.*, Int. J. Mod. Phys. B **14**, 2725 (2000).
[17] S. Yoon *et al.*, Phys. Rev. B **58**, 2795 (1998).
[18] A. Lanzara *et al.*, Phys. Rev. Lett. **81**, 878 (1998).
[19] A. Moro, S. Yunoki, and E. Dagotto, Science **283**, 2034 (1999).
[20] J. M. De Teresa *et al.*, Nature (London) **386**, 256 (1997).
[21] J. J. Neumeier, M. F. Hundley, J. D. Thompson, and R. H. Heffner, Phys. Rev. B **52**, 7006 (1995).
[22] H. Y. Hwang, T. T. M. Palstra, S. W. Cheong, and B. Batlogg, Phys. Rev. B **52**, 15 046 (1995).
[23] Y. Moritomo, A. Asamitsu, and Y. Tokura, Phys. Rev. B **51**, 16 491 (1995).
[24] V. Laukhin, J. Fontcuberta, J. L. Garcia-Munoz, and X. Obradors, Phys. Rev. B **56**, 10 009 (1997).
[25] R. Senis *et al.*, Phys. Rev. B **57**, 14 680 (1998).
[26] A. Nossov *et al.*, Eur. Phys. J. B **6**, 467 (1998).
[27] A. Congeduti *et al.*, Phys. Rev. Lett. **86**, 1251 (2001).
[28] A. Congeduti *et al.*, Phys. Rev. B **63**, 184410 (2001).
[29] J. Wittig, Z. Phys. B: Condens. Matter **38**, 11 (1980).
[30] M. Nuñez-Reguero and C. Acha, *Studies on High Tc Superconductors* (Nova Science, Commack, NY, 2000), Vol. 24.
[31] H. K. Mao, J. Xu, and P. M. Bell, J. Geophys. Res. **91**, 4673 (1986).
[32] A. P. Hammersley *et al.*, High Press. Res. **14**, 235 (1996).
[33] A. C. Larsson and R. B. von Dreele, General Structure Analysis System (GSAS), Los Alamos National Laboratory, Rep. LAUR 86-748, 2000.
[34] F. J. Birch, J. Geophys. Res. **91**, 4949 (1986).